PAPER

One pot synthesis of Fe₃O₄/MnO₂ core–shell structured nanocomposites and their application as microwave absorbers

Xianguo Liu,*[a] Niandu Wu,[a] Caiyun Cui,[a] Nannan Bi[a] and Yuping Sun[b]

Fe₃O₄/MnO₂ core–shell structured nanocomposites have been synthesized by a one-pot approach at ambient temperature and pressure. The morphology of the prepared Fe₃O₄/MnO₂ nanoparticles is governed by the Mn/Fe molar ratio in the precursor. When the molar ratio of Mn/Fe is 1 : 10, the nanocomposites exhibit a special microstructure, in which MnO₂ nanorods are formed on the surface of spherical Fe₃O₄ nanoparticles. With the increase of the Mn/Fe ratio to 1 : 2, core–shell structured nanoparticles with Fe₃O₄ nanoparticles as cores and MnO₂ as the shell are obtained. The microwave absorption properties of the core–shell Fe₃O₄/MnO₂ nanocomposites were studied in the 2–18 GHz frequency range. The microwave absorption performance of the Fe₃O₄/MnO₂ nanocomposites exhibited a remarkable enhancement in comparison with pure Fe₃O₄ nanoparticles, ascribed to the fact that MnO₂ nanostructures can improve the dielectric loss factor and the electromagnetic (EM) matching degree. The absorption peaks of the Fe₃O₄/MnO₂–paraffin composites are red shifted compared to those of Fe₃O₄–paraffin composites. Due to the MnO₂ nanorods on the surface of the Fe₃O₄ nanoparticles, the produced microcurrent can reduce the electron transition energy and lead to better microwave absorption by the Fe₃O₄ nanoparticle/MnO₂ nanorod nanocomposites.

1. Introduction

Serious electromagnetic (EM) interference problems arising from rapidly expanding communication devices, such as wireless internet, mobile telephones and military application devices, have sparked a large interest towards research on EM wave loss materials. EM wave loss materials can absorb energy from EM waves and convert the EM energy to thermal energy through the combined action of dielectric loss and magnetic loss.[1–5] For their application, it is desirable to achieve a strong EM wave absorption (99% absorption) in the whole 2–18 GHz range for a thin absorber layer with low mass density. The EM wave loss performance can be determined by the complex permeability/permittivity, EM impedance matching and the microstructure of the absorbents.[2] Many efforts have been made on the fabrication of various microwave absorption materials. Nanocomposites consisting of magnetic metals and dielectric materials have attracted extensive interest in microwave absorption in the 2–18 GHz range.[6–10]

For certain severe working environments in aerospace industry or for devices for high-temperature applications,

[a]*School of Materials Science and Engineering, Anhui University of Technology, Maanshan, 243002, China. E-mail: liuxianguohugh@gmail.com; Fax: +86 555 2311570; Tel: +86 555 2311570*

[b]*Center for Engineering Practice and Innovation Education, Anhui University of Technology, Maanshan, 243032, China*

development of EM wave materials with strong anti-oxidation abilities is needed. At this point, both metals and carbon-based materials could be oxidized when applied to high-temperature working environments, resulting in the degradation of the EM absorption performance. To develop EM wave absorption materials for high-temperature applications, thermal stability is highly required. Basic EM absorption mechanisms suggest that good absorbers should have mobile charge carriers for absorption.[11,12] At this point, charge carriers in semiconductors could be excited at elevated temperatures, leading to an increase in charge carriers at high temperature. Therefore, semiconductor oxides seem to be good candidates for EM wave absorbers at high temperature.

As a typical semiconductor oxide, MnO₂ is an attractive class of dielectric absorption material with broad frequency bandwidth . Its wave attenuation properties can be attributed mainly to its high dielectric constant. Meanwhile, MnO₂ also possesses the advantages of cheap and natural abundance, and environmental friendliness.[13] So far, numerous studies on the EM properties of MnO₂ materials have been reported, including nanowires, nanorods, microspheres, and hierarchical structures.[14–17] MnO₂ urchin-like nanostructures exhibit a good microwave absorption performance in the frequency range of 2–18 GHz.[16] Guan *et al.* have studied the dielectric and EM characteristics of MnO₂ materials with different crystalline and morphological structures prepared through different methods.[13,16] Due to their superior properties of large magnetic

loss and great resistivity, Fe_3O_4-based nanocomposites have been widely prepared and their EM absorption performance has been deeply investigated.[18–20] However, the EM absorption performance of Fe_3O_4/MnO_2 nanocomposites has been rarely studied.

In this work, a series of Fe_3O_4/MnO_2 nanocomposites were synthesized at 90 °C by a facile and green one pot hydrothermal method through the adjustment of the molar ratio of Mn/Fe (0 : 10, 1 : 10, and 1 : 2). Inexpensive $FeSO_4$ and $KMnO_4$ were applied as the precursors of Fe and Mn, respectively. Moreover, the morphology could be controlled through the adjustment of the molar ratio of Mn/Fe. The morphology, microstructure, and microwave absorption properties of these nanocomposites have been investigated systematically and the effects of the MnO_2 component are discussed.

2. Experimental

2.1 Synthesis of Fe_3O_4/MnO_2 nanocomposites

A hydrothermal method was used to fabricate the core–shell structured nanocapsules with initial Mn/Fe molar ratios of 0 : 10 (sample 1), 1 : 10 (sample 2) and 1 : 2 (sample 3) at 90 °C with continuous gentle stirring. $FeSO_4 \cdot 7H_2O$ (2.5 mmol) was dissolved in 100 mL deionized water and kept for 1 h. Then, 1 mL of 5.0 M NaOH was added to the solution, generating a green suspension. Then, an aqueous solution of $KMnO_4$ was added into the reaction solution dropwise, producing a dark brown precipitate. After aging the dark brown precipitate for 12 h, the Fe_3O_4/MnO_2 nanocomposites were finally obtained, thoroughly washed with deionized water and ethanol alternately, and then dried in a vacuum drying oven at 60 °C.

2.2 Material characterization

The phase, morphology and microstructure of the products were characterized by X-ray diffraction (XRD, Brucker D8 Advance diffractometer), scanning electron microscopy (SEM, JEOL-6300F) equipped with an energy dispersive spectrometer (EDS, Oxford, UK) and high-resolution transmission electron microscopy (HRTEM, JEOL-2010F) at an acceleration voltage of 200 kV, respectively.

2.3 Electromagnetic absorption measurements

The details on the EM measurements of the samples have been described elsewhere.[2–4] The mass ratio of the products in the paraffin-bonded composites was set to be 40 wt%. The complex permittivity (ε_r) and the complex permeability (μ_r) of the composites were obtained in a frequency (f) range of 2 to 18 GHz using an Agilent 8722ES network analyzer. ε_r and μ_r were calculated from the S-parameters tested by the calibrated vector network analyzer, using a simulation program with the Reflection/Transmission Nicolson–Ross model.

3. Results and discussion

Fig. 1 shows the XRD patterns of the three as-synthesized samples. For the three samples, the XRD patterns show
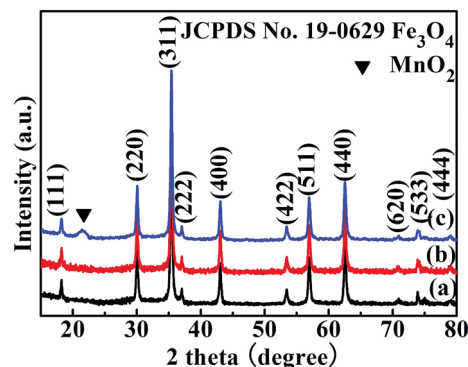

Fig. 1 XRD patterns of (a) sample 1, (b) sample 2 and (c) sample 3.

reflections at (111), (220), (311), (222), (400), (422), (511), (440), (620), (533) and (444) that can be readily indexed to magnetite Fe_3O_4 [JCPDS Card no: 19-0629] with a space group of $Fd\bar{3}m$. No peaks for MnO_2 in sample 2 are observed due to its small amount and the breaking down of the periodic boundary condition on the surface of Fe_3O_4 nanoparticles.[21] An amorphous peak located at 21.4° in sample 3 indicates the existence of amorphous MnO_2. The MnO_2 structure in sample 2 and sample 3 was further confirmed by the HRTEM analysis later in the paper.

As shown in Fig. 2(a)–(c), the typical morphology of the three samples was examined using SEM. For sample 1 (Fig. 2(a)), it can be seen that the bare spheres with smooth surface have an average size of about 40 nm. Once $KMnO_4$ (Mn/Fe molar ratios of 1 : 10) is added (sample 2), some nanorods with a length of about 15 nm and diameter of about 5 nm are formed and anchored on the surface of the nanospheres with an averaged size of 40 nm (Fig. 2(b)). With the increase of the Mn/Fe molar ratio to 1 : 2 (sample 3), the product exhibits a spherical shape with an average size of 60 nm (Fig. 2(c)), which is larger than
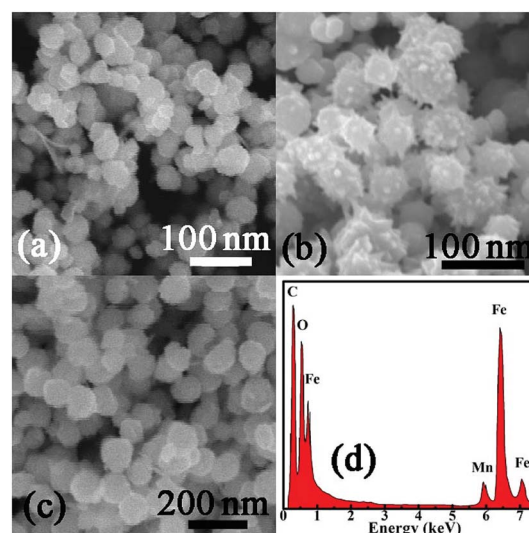

Fig. 2 SEM images of (a) sample 1, (b) sample 2 and (c) sample 3. (d) EDS spectrum of sample 3.

that of sample 1. In order to discriminate between sample 1 and sample 3, EDS spectroscopy (Fig. 2(d)) was used to further evidence the elemental composition. It is clearly seen that Mn is present in sample 3, which is in good agreement with the XRD results. The detailed microstructure of these three samples was further investigated by HRTEM. It is obvious that no core–shell type microstructure can be observed in the HRTEM image of sample 1 (Fig. 3(a)). The lattice plane spacing of the nanoparticles is about 0.253 nm, which corresponds to the (311) plane of Fe_3O_4. Fig. 3(b) demonstrates the typical HRTEM image of sample 2. A single nanorod is clearly seen on the surface of a Fe_3O_4 nanoparticle. As shown in the inset of Fig. 3(b), the measured interplanar distance of 0.41 nm in the nanorod can be assigned to the characteristic interplanar distance of (131) of MnO_2. The HRTEM image in Fig. 3(c) reveals the nanocomposites in sample 3 own a core–shell type structure consisting of an inner Fe_3O_4 nanoparticle core encapsulated by an amorphous shell with thickness of about 10 nm. The amorphous shell should be MnO_2 on the basis of the XRD spectra, the EDS results and the experiment process. Except for the MnO_2 shell, the size of the Fe_3O_4 nanoparticle core in sample 3 is equal to that of sample 1.

On the basis of the above experimental results and the literature, the synthetic process for the Fe_3O_4/MnO_2 nanocomposites is proposed, as schemed in Fig. 4. For the three samples, the mechanism of formation of green $Fe(OH)_2$ follows eqn (1). For the synthesis of sample 1, $Fe(OH)_2$ is oxidized to ferric hydroxide by oxygen dissolved in the solution (eqn (2)), and the formation of Fe_3O_4 nanoparticles is achieved through a dehydration reaction of ferrous hydroxide and ferric hydroxide (eqn (3)).[22] For samples 2 and 3, redox reactions between $Fe(OH)_2$ and $KMnO_4$ take place rapidly with the formation of dark sediments once $KMnO_4$ is added to the green $Fe(OH)_2$ suspension (eqn (4)).[22] Fe_3O_4 is a well-known ferrimagnetic oxide and MnO_2 is a diluted magnetic semiconductor. At the initial stage of sample 2 with a Mn/Fe ratio of 1 : 10, the generated MnO_2 nanoparticles are randomly adhered onto the surface of the Fe_3O_4 nanoparticles, due to the isotropic magnetic field of spherical Fe_3O_4 nanoparticles. Afterward, the distribution of the magnetic field is changed. Because the size of the MnO_2 nanoparticles simulated from the MnO_2 nanorods (5 nm) is smaller than that of Fe_3O_4 nanoparticles (40 nm), a tip effect promotes the adhesion of MnO_2 nanoparticles to the MnO_2 nanoparticles on the surface of the Fe_3O_4 nanoparticles. Due to the ferromagnetic nature of Fe_3O_4, this tip effect is
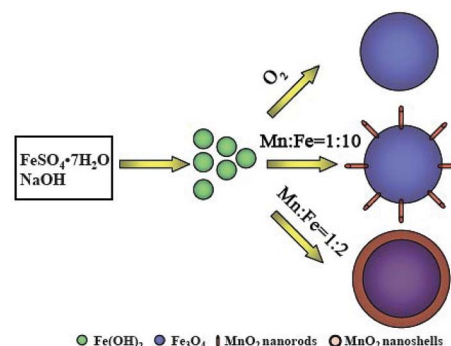
Fig. 4 Schematic illustration of the formation of Fe_3O_4/MnO_2 nanocomposites.

weakened with the length of rod-like nanostructures. For the formation of core–shell structured Fe_3O_4/MnO_2 nanocomposites (sample 3), the Mn/Fe ratio of 1 : 2 exceeds the reaction molar ratio in eqn (4). The excess of $KMnO_4$ is slowly decomposed to MnO_2 under neutral or alkaline conditions (eqn (5)).[23] Zhang et al. reported that MnO_2 has a substantial number of hydroxyl radicals on the surface and a high affinity for Fe.[22] Therefore, MnO_2 nanoparticles tend to settle on the surface of the Fe_3O_4 nanoparticles forming nanoshells.

$$FeSO_4 + 2NaOH \rightarrow Fe(OH)_2 + Na_2SO_4 \quad (1)$$

$$3Fe(OH)_2 + 1/2O_2 \rightarrow Fe(OH)_2 + 2FeOOH + H_2O \quad (2)$$

$$Fe(OH)_2 + 2FeOOH \rightarrow Fe_3O_4 + 2H_2O \quad (3)$$

$$9Fe(OH)_2 + 2KMnO_4 \rightarrow 3Fe_3O_4 + 2MnO_2 + 2KOH + 8H_2O \quad (4)$$

$$4KMnO_4 + 2H_2O \rightarrow 4MnO_2 + 3O_2 + 4KOH \quad (5)$$

According to the transmit-line theory, the absorption characteristics of materials depend on a number of factors, including the frequency (f), sample thickness (d), relative complex permittivity ($\varepsilon_r = \varepsilon' - j\varepsilon''$) and relative complex permeability ($\mu_r = \mu' - j\mu''$). In order to investigate the effect on the EM wave absorption of the three samples, the EM parameters of paraffin-bonded 40 wt% sample composites were measured at room temperature in the frequency range 2–18 GHz. According to Fig. 5(a), both real (ε') and imaginary (ε'') parts of ε_r of the three sample–paraffin composites exhibit a similar tendency, i.e., declining significantly from 2 to 6 GHz and then decreasing slightly at higher frequencies. The phenomena can be ascribed to an increased lagging of the dipole-polarization response with respect to the electric field change at high frequencies.[24] However, compared to those of the Fe_3O_4 nanoparticles–paraffin composite, both ε' and ε'' components of ε_r increase with the Mn/Fe ratio, which is similar to those of Fe/MnO_2 composites.[25] According to the free electron theory, $\varepsilon'' = \sigma/(2\pi f \varepsilon_0)$,[26] where σ is the electrical conductivity, the high ε'' values for Fe_3O_4/MnO_2 nanocomposites at 2–18 GHz are indicative of high electrical conductivities, attributed to an
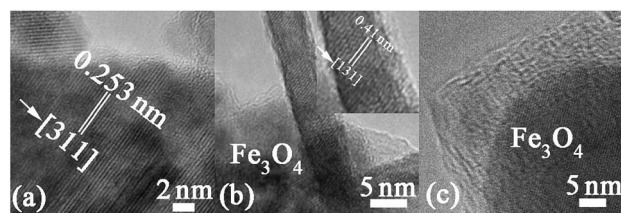

Fig. 3 HRTEM images of (a) sample 1, (b) sample 2 and (c) sample 3. The inset in panel (b) is the typical HRTEM image of a nanorod in sample 2.
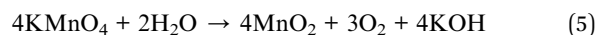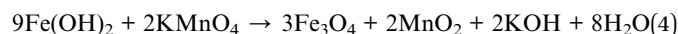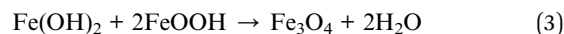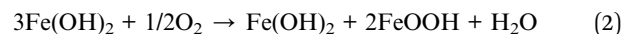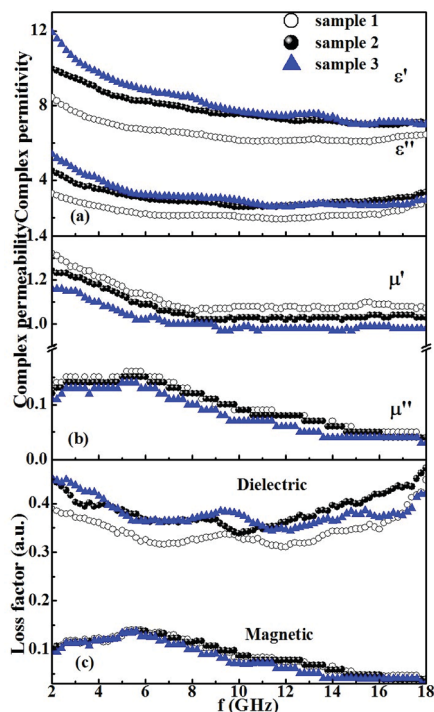
Fig. 5 (a) Complex permittivity, (b) complex permeability and (c) dielectric loss factor and magnetic loss factor of the three sample–paraffin composites.

enhancement due to the MnO_2 nanostructures on the surface of Fe_3O_4 nanoparticles. MnO_2 itself is a dielectric material with a permittivity as high as 16.[13] Therefore, by adding MnO_2, an increased dielectric loss can be achieved in the Fe_3O_4/MnO_2 nanocomposites.

The frequency dependence on the real part (μ') and the imaginary part (μ'') of μ_r of the three sample–paraffin composites is shown in Fig. 5(b). μ' curves display a similar tendency, decreasing as the frequency increases from 2 to 18 GHz. In addition, the value of μ' is reduced with the increase in the Mn/Fe ratio. The decrease in μ' for the Fe_3O_4/MnO_2–paraffin composite can be explained by the introduction of the paramagnetic MnO_2 component in the Fe_3O_4/MnO_2 nanocomposites. Compared to the variation of μ', there is no clear difference between the μ'' values of the different samples, and the μ'' curves almost coincide. It can be found that a broad resonance peak around 3–6 GHz appears in the curves of μ'' and the resonance frequency remains almost unvaried with the Mn/Fe ratio. As it is known, resonance frequencies depend strongly on the effective anisotropy field, which is associated with magneto-crystalline anisotropy, on the magnetic-particle size and on the magnetic-particle geometry.[27,28] For the as-prepared three samples, the Fe_3O_4 nanoparticles maintain a similar size distribution and morphology, which explains why the resonance frequency remains almost unvaried.

The real and imaginary parts of the EM parameters correspond to the energy storage and loss of EM waves in the propagation process, respectively. The dielectric loss factor (tan $\delta_E = \varepsilon''/\varepsilon'$) and magnetic loss factor (tan $\delta_M = \mu''/\mu'$) are commonly used to

describe EM loss capacity, which can be influenced by either fillers in the composites or artificially periodic architectures.[1] As shown in Fig. 5(c), the magnetic loss factor curves of the three sample–paraffin composites are almost overlapped. On the other hand, the dielectric loss of the Fe_3O_4/MnO_2–paraffin composites is larger than that of the Fe_3O_4–paraffin composite over the whole 2–18 GHz range. According to the EM loss model, Fe_3O_4/MnO_2 nanocomposites may exhibit a better microwave absorption performance than pure Fe_3O_4 nanoparticles in the whole frequency range 2–18 GHz. From the dielectric loss curves of sample 2 and sample 3, we can extract the following observations: (1) the dielectric loss of sample 3 is larger than that of sample 2 below 4 GHz; (2) the dielectric loss curves for the two samples basically overlap in the frequency range 4–9 GHz; (3) the dielectric loss of sample 3 is still larger than that of sample 2 in 9–11 GHz; and (4) the dielectric loss of sample 2 exceeds that of sample 3 between 11 and 18 GHz.

Microwave absorption can be further quantitatively evaluated by the value of the reflection loss (RL), in which −20 dB is equivalent to 99% efficiency of microwave absorption. From the ε_r and μ_r values obtained using the Matlab, RL is calculated by using the formula of transmission lines,[2]

$$Z_{in} = Z_0(\mu_r/\varepsilon_r)^{1/2} \tanh[j(2\pi fd/c)(\mu_r\varepsilon_r)^{1/2}] \quad (6)$$

$$RL = 20\log|(Z_{in} - Z_0)/(Z_{in} + Z_0)|, \quad (7)$$

where Z_0 is the impedance of free space, Z_{in} is the input impedance of the absorber, and c is the velocity of EM waves in free space.

The RL curves of the three composites with a thickness range of 1.5–5.0 mm can be calculated according to eqn (6) and (7), and the results are shown in Fig. 6. The common characteristic for the three composites is that the RL peak shifts to a lower frequency with the increase in thickness. However, the RL peak intensity and required peak frequency at the same thickness are different. Fig. 6(a) shows that the RL value of the sample 1–paraffin composite are smaller than those of composites including samples 2 and 3 at the same absorber thickness. For example, the optimal RL value of the sample 1–paraffin composite with a thickness of 1.7 mm is −27.9 dB at 17.6 GHz, while the RL value of the sample 2–paraffin composite is −41.5 dB at 16.8 GHz (Fig. 6(b)), and that of the sample 3–paraffin composite is −29.3 dB at 17.4 GHz (Fig. 6(c)) for the same thickness. It is interesting that the RL peak (exceeding −25 dB) of three composites is located at 17–18 GHz due to the increase of the dielectric loss factor at 17–18 GHz (Fig. 5(c)). Compared to the sample 1–paraffin composite, the absorption peak of the sample 2–paraffin and sample 3–paraffin composites at the same thickness have shifted to a lower frequency, *i.e.*, red shifted. This effect is similar to those of Ni/(C, silicides) nanocapsules, FeCo/C/BaTiO$_3$ nanocapsules and Ag-coated the Co$_2$Z barium ferrite composites, in which charge transfer at the interface give rise to an electric dipole.[29–31] Fig. 7 presents the difference of the RL peak positions for sample 2–paraffin and sample 3–paraffin composites relative to that of the sample 1–paraffin composite at different thicknesses of the absorber.
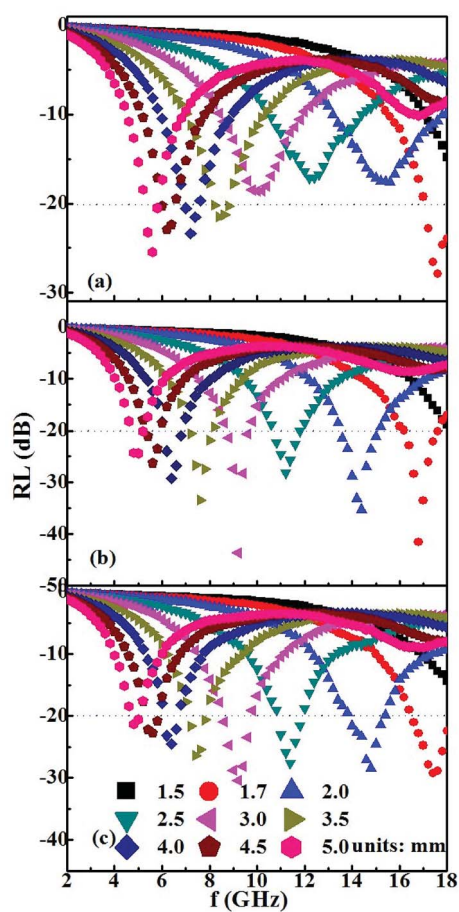
Fig. 6 Calculated RL curves for (a) sample 1–paraffin, (b) sample 2–paraffin and (c) sample 3–paraffin composites.
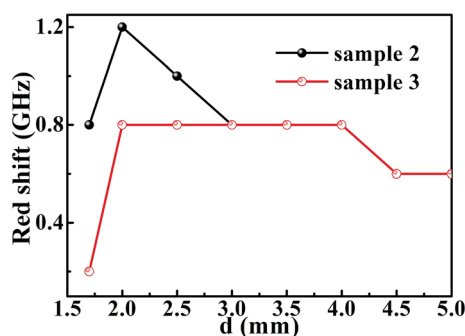

Fig. 7 Red shift value of the maximum RL peak position for sample 2–paraffin and sample 3–paraffin composites, relative to that of sample 1–parafin composite.

The red shift extent of the sample 2–paraffin composite is larger than that of the sample 3–paraffin composite as the thickness increases from 1.7 to 2.5 mm. The red shift value of paraffin-bonded composites with sample 2 and sample 3 are overlapped when the thickness is 3.0–5.0 mm.

When an EM wave penetrates into the absorbent, the wave is absorbed through electron transitions. MnO_2 nanostructures

can cause the localization of electron density and generate additional energy levels near the Fermi level, which may reduce the electron transition energy.[30] Because of the reduction of the electron transition energy, the transition can occur at a lower frequency, which leads to a red shift of the absorption peak at different thicknesses of the absorption layer. The difference between sample 2–paraffin and sample 3–paraffin composites is ascribed to their different geometrical morphology. MnO_2 nanorods on the surface of Fe_3O_4 nanoparticles allow a micro-network to be formed.[31] A microcurrent can be produced in the frame of the micronetwork, which can further reduce the electron transition energy.[32] Hence, the red shift value for the sample 2–paraffin composite is larger than that for the sample 3–paraffin composite when the thickness is thinner than 3.0 mm. However, with the increasing thickness, the micronetwork is destroyed by the paraffin and the sample preparation procedure. Hence, the red shift curves coincide at thicknesses smaller than 3.0 mm.

As shown in Fig. 6(b) and (c), it is worth noting that the RL peak values for the sample 2–paraffin and sample 3–paraffin composites are both obtained at the same frequency and the same thickness, at thicknesses larger than 3.0 mm. The phenomena may be ascribed to the overlapped dielectric loss and magnetic loss in the frequency range 5–9 GHz. However, compared to the sample 2–paraffin composite, the sample 3–paraffin composite exhibits a lower RL value at different absorbent layer thicknesses as seen in Fig. 6(b) and (c), which cannot be explained reasonably by the EM loss model. The optimal RL value (−43.6 dB) of the sample 2–paraffin composite is larger than that of the sample 3–paraffin composite at 9.2 GHz with thickness of 3.0 mm (−30.5 dB). For magnetic/dielectric-loss absorbers, an excellent microwave absorption performance mainly results from proper EM impedance matching. In order to effectively estimate the EM impedance matching degree, a delta-function method has been proposed.[33] The delta-function can be described as,

$$\varDelta = |\sinh^2(Kfd) - M|,$$

where K and M are determined by ε_r and μ_r. The delta value should reach zero when RL approaches minus infinity. The smaller the delta value, the better the EM impedance matching. According to the measured ε_r and μ_r values, the calculated delta maps of the three sample–paraffin composites are shown in Fig. 8. The blue area for the Fe_3O_4/MnO_2–paraffin composite is obviously larger than that of the Fe_3O_4–paraffin composite. The dark blue area of the Fe_3O_4/MnO_2 nanorod–paraffin composite (4.466) slightly exceeds that of the Fe_3O_4/MnO_2 nanoshell–paraffin composite (4.437), which can explain the reasons behind the enhanced microwave absorption ability of Fe_3O_4/MnO_2 nanorods. The RL and the delta values exhibit the same tendency, indicating that the enhanced microwave absorption performance of the Fe_3O_4/MnO_2–paraffin composite results from a good EM impedance matching through the special microstructure. Compared to the pure Fe_3O_4–paraffin composite, the remarkable enhancement on the microwave absorption performance of the Fe_3O_4/MnO_2–paraffin composite

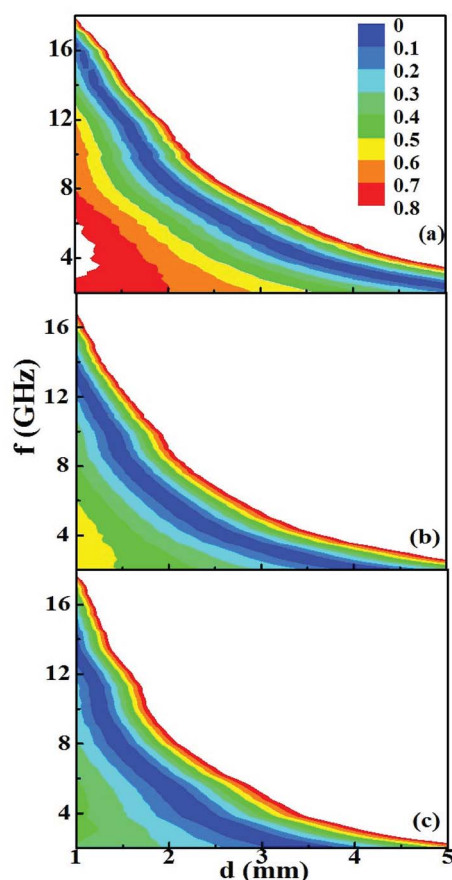Fig. 8 Calculated delta value maps of the paraffin-bonded composites with (a) sample 1, (b) sample 2 and (c) sample 3.

paraffin composite can be attributed to the increase of ε_r and the dielectric loss factor, and proper EM matching. When MnO_2 nanostructures are introduced into the Fe_3O_4/MnO_2 nanocomposites, the absorption peaks of the Fe_3O_4/MnO_2–paraffin composites red shift compared to those of Fe_3O_4–paraffin composites. The MnO_2 nanorods on the surface of the Fe_3O_4 nanoparticles allow a micronetwork to be formed. A microcurrent can be produced in the frame of the micronetwork, which can further reduce the electron transition energy. This special microstructure contributes to the enhanced microwave absorption properties of the Fe_3O_4 nanoparticle/MnO_2 nanorod nanocomposites. As a result, Fe_3O_4/MnO_2 nanocomposites are attractive candidates as EM wave absorbers.

Acknowledgements

Notes and references

1 X. F. Zhang, P. F. Guan and J. J. Guo, *Part. Part. Syst. Charact.*, 2013, **30**, 842–846.
2 J. J. Jiang, D. Li, D. Y. Geng, J. An, J. He, W. Liu and Z. D. Zhang, *Nanoscale*, 2014, **6**, 3967–3971.
3 X. G. Liu, Q. Z. Ou, D. Y. Geng, Z. Han, Z. G. Xie and Z. D. Zhang, *J. Phys. D: Appl. Phys.*, 2009, **42**, 155004.
4 X. F. Zhang, J. J. Guo and G. W. Qin, *Appl. Phys. Lett.*, 2014, **104**, 252404.
5 D. Micheli, A. Vricella, R. Pastore and M. Marchetti, *Carbon*, 2014, **77**, 756–774.
6 A. B. Zhang, S. T. Liu, K. K. Yan, Y. Ye and X. G. Chen, *RSC Adv.*, 2014, **4**, 12565–13568.
7 H. M. Xiao and S. Y. Fu, *CrystEngComm*, 2014, **16**, 2097–2112.
8 S. Ryu, C. B. Mo, H. Lee and S. H. Hong, *J. Nanosci. Nanotechnol.*, 2013, **13**, 7669–7674.
9 X. G. Liu, S. W. Or, S. L. Ho, C. C. Cheung, C. M. Leung, Z. Han, D. Y. Geng and Z. D. Zhang, *J. Alloys Compd.*, 2011, **509**, 9071–9075.
10 Y. Li, J. Zhang, Z. W. Liu, M. M. Liu, H. J. Lin and R. C. Che, *J. Mater. Chem. C*, 2014, **2**, 5216–5222.
11 W. L. Song, M. S. Cao, Z. L. Hou, M. M. Lu, C. Y. Wang, J. Yuan and L. Z. Fan, *Appl. Phys. A: Mater. Sci. Process.*, 2014, **116**, 1779–1783.
12 M. H. Al-Saleh and U. Sundararaj, *Carbon*, 2009, **47**, 1738–1746.
13 H. T. Guan, J. B. Xie, G. Chen and Y. D. Wang, *Mater. Chem. Phys.*, 2014, **143**, 1061–1068.
14 S. F. Chin, S. C. Pang and M. A. Anderson, *Mater. Lett.*, 2010, **64**, 2670–2672.
15 X. L. Shi, M. S. Cao, X. Y. Fang, J. Yuan, Y. Q. Kang and W. L. Song, *Appl. Phys. Lett.*, 2008, **93**, 223112.
16 Y. P. Guan, J. Zhang, H. Jing and S. H. Liu, *J. Solid State Chem.*, 2011, **184**, 1165–1171.
17 M. Zhou, X. Zhang, L. Wang, J. M. Wei, L. Wang, K. W. Zhu and B. X. Feng, *Mater. Chem. Phys.*, 2011, **130**, 1191–1194.

should be attributed to the increase of ε_r and the dielectric loss factor, and the proper EM matching induced by the special microstructure. Moreover, due to the MnO_2 nanorods on the surface of Fe_3O_4 nanoparticles, the produced microcurrent can reduce the electron transition energy, which contributes to the improved microwave absorption ability of the Fe_3O_4/MnO_2 nanorod nanocomposites.

4. Conclusions

In summary, Fe_3O_4/MnO_2 nanocomposites have been synthesized by a simple and environmentally friendly method. The morphology of the prepared Fe_3O_4/MnO_2 nanocomposites is governed by the optimisation of the molar ratio of Mn/Fe in the precursor. When the molar ratio of Mn/Fe is 1 : 10, the prepared nanocomposites display a special microstructure, in which MnO_2 nanorods are formed on the surface of spherical Fe_3O_4 nanoparticles. By increasing the Mn/Fe ratio to 1 : 2, core–shell structured nanocomposites with Fe_3O_4 nanoparticles as cores and MnO_2 as the shell are obtained. The formation mechanism of Fe_3O_4/MnO_2 nanocomposites has been proposed based on XRD, SEM and TEM results. Compared to the pure Fe_3O_4–paraffin composite, the remarkable enhancement on the microwave absorption performance of the Fe_3O_4/MnO_2–

18 M. Z. Xu, X. L. Shi, X. Q. Zou, H. Pan, M. D. Liu, K. Jia and X. B. Liu, *J. Magn. Magn. Mater.*, 2014, **371**, 20–28.

19 Y. P. Sun, F. Xiao, X. G. Liu, C. Feng and C. G. Jin, *RSC Adv.*, 2013, **3**, 22554–22559.

20 L. N. Wang, X. L. Jia, Y. F. Li, F. Yang, L. Q. Zhang, L. P. Liu, X. Ren and H. T. Yang, *J. Mater. Chem. A*, 2014, **2**, 14940–14946.

21 Y. P. Sun, X. G. Liu, C. Feng, J. C. Fan, Y. H. Lv, Y. R. Wang and C. T. Li, *J. Alloys Compd.*, 2014, **586**, 688–692.

22 Z. W. Zhao, J. Liu, F. Y. Gui, H. Feng and L. L. Zhang, *J. Mater. Chem.*, 2012, **22**, 9052–9057.

23 R. Deng, X. Xie, M. Vendrell, Y. T. Chang and X. Liu, *J. Am. Chem. Soc.*, 2011, **133**, 20168–20171.

24 H. Wang, H. H. Guo, Y. Y. Dai, D. Y. Geng, Z. Han, D. Li, T. Yang, S. Ma, W. Liu and Z. D. Zhang, *Appl. Phys. Lett.*, 2012, **101**, 083116.

25 W. Q. Zhang, S. W. Bie, H. C. Chen, Y. Lu and J. J. Jiang, *J. Magn. Magn. Mater.*, 2014, **358–359**, 1–4.

26 T. Draine and P. J. Flatau, *J. Opt. Soc. Am. A*, 1994, **11**, 1491–1495.

27 F. Ma, Y. Qin and Y. Z. Li, *Appl. Phys. Lett.*, 2010, **96**, 202507.

28 H. Wang, Y. Y. Dai, W. J. Gong, D. Y. Geng, S. Ma, D. Li, W. Liu and Z. D. Zhang, *Appl. Phys. Lett.*, 2013, **102**, 223113.

29 J. J. Jiang, H. Wang, H. H. Guo, T. Yang, W. S. Tang, D. Li, S. Ma, D. Y. Geng, W. Liu and Z. D. Zhang, *Nanoscale Res. Lett.*, 2012, **7**, 238.

30 Y. B. Zhang, F. Xu, G. G. Tan, J. L. Zhang, T. Wang and F. S. Li, *J. Alloys Compd.*, 2014, **615**, 749–753.

31 M. S. Cao, X. L. Shi, X. Y. Fang, H. B. Jin, Z. L. Hou and W. Zhou, *Appl. Phys. Lett.*, 2007, **91**, 203110.

32 P. C. P. Watts, W. K. Hsu, A. Barnes and B. Chambers, *Adv. Mater.*, 2003, **15**, 600–602.

33 Z. Ma, C. T. Cao, Q. F. Liu and J. B. Wang, *Chin. Phys. Lett.*, 2012, **29**, 038401.